Intraflagellar transport-20 guides the ciliary membrane trafficking of channelrhodopsin in *Chlamydomonas reinhardtii*

Alka Kumari[1], Shilpa Mohanty[1], Snigdha Samanta[1] and Suneel Kateriya[1*]

Laboratory of Optobiotechnology, School of Biotechnology, Jawaharlal Nehru University, New Delhi, India.

*To whom correspondence should be addressed.

Corresponding authors' e-mail: skateriya@jnu.ac.in

†ORCID identifiers: S.K. 0000-0001-5428-4297

Abstract

The primary cilium is a microtubule-based organelle essential for cellular signaling, whose assembly depends on intraflagellar transport (IFT). IFT20, a unique IFT-B component, localizes to both Golgi and cilium/flagellum, suggesting a role in membrane trafficking. Here, we analyzed CrIFT20-mediated ciliary membrane trafficking of channelrhodopsin-1 (ChR1) in *Chlamydomonas reinhardtii*. Spectroscopic analysis shows recombinant CrIFT20 has a predominantly helical structure and undergoes GTP-dependent shuttle conformational change. Co-immunolocalization of IFT20 in wild-type *C. reinhardtii* shows puncta distribution throughout cilia and co-localizes directly/indirectly with ChR1 in cilia. Further co-immunoprecipitation supports the cellular biochemical evidence that IFT20 guides the trafficking of ChR1 at the ciliary membrane. Protein interaction network analysis reveals that IFT20 serves as a central adaptor interfacing early ciliary trafficking components with IFT-B complex and BBSome subunits. These findings extend the mechanistic understanding of ciliary membrane protein delivery in *C. reinhardtii* and reveal a conserved role of IFT20 in photoreceptor trafficking. This study illustrates how coordinated adaptor, motor, and cargo selection maintain the ciliary distribution of ciliary membrane proteins. This study aids in delineating the underlying mechanism of protein trafficking in cilia using *C. reinhardtii* as a model system, crucial for studying human cilia-associated disorders (ciliopathies).

Keywords: Intraflagellar transport-20, Channelrhodopsin-1, ciliary membrane trafficking, *Chlamydomonas reinhardtii*.

1. Introduction

The primary cilium is a non-motile, microtubule-based projection that functions as a sensory antenna for extracellular signals. Its structure and function rely on precisely regulated trafficking pathways that direct membrane proteins and signaling molecules from the cytoplasm and Golgi to the ciliary compartment (Ernst et al., 2014; Satir et al., 2010; Wingfield et al., 2018). Delivery is governed by specific targeting motifs, such as the VxPx sequence in rhodopsin, and by coordinated vesicular transport orchestrated through Rab GTPases, Arfs, and the intraflagellar transport (IFT) machinery (Leroux et al., 2007; Deretic, D., 2005; Hanke-Gogokhia et al., 2016; Ward et al., 2011). Hence, any of these processes are disrupted, core signaling pathways break down, leading to a diverse group of developmental and sensory disorders known as ciliopathies (Fliegauf et al., 2007; Reiter et al., 2017; Mill et al., 2023).

Central to ciliary assembly and homeostasis is the IFT system, a multi-subunit transport machinery composed of two major complexes (Lechtreck et al., 2015; Jiang et al., 2023). Intraflagellar transport (IFT) is a highly coordinated process that drives the bidirectional movement of protein complexes along the ciliary axoneme. The IFT-B complex mediates anterograde transport toward the ciliary tip through the activity of the kinesin-2 motor, whereas the IFT-A complex facilitates retrograde transport of IFT particles and associated cargo back to the cell body via dynein-2 (Morthorst et al., 2018; Wang et al., 2018; Taschner et al., 2016; Pazour et al., 2012). In contrast to most IFT proteins, which are mainly confined to the basal body and cilium, IFT20 is also found at the Golgi apparatus in addition to the basal body and the ciliary transition zone (Follit et al., 2008). This dual localization enables IFT20 to serve as a critical link between post-Golgi vesicular trafficking and the targeting of cargo proteins to the cilium.

This process depends on coordinated interactions with members of the Arf and Rab families of small GTPases (Deretic et al., 2013). In particular, Arf4 contributes to cargo sorting at the Golgi by recognizing ciliary targeting signals and promoting the formation of transport vesicles carrying ciliary proteins (Deretic et al., 2021). Rab11 and Rab8 GTPases are involved in the transport, docking, and fusion of IFT20-containing vesicles at the periciliary membrane through the Rab11–Rabin8–Rab8 cascade (Saha et al., 2024; Blacque et al., 2018). At this site, IFT20 associates with the IFT-B complex and participates in cargo loading and sorting before anterograde transport along the axoneme by kinesin-2 (Baker et al., 2003). Any

interruption in these processes be it in Arf/Rab regulation, the function of the IFT20 adaptor, or the integrity of the IFT complex leads to flawed ciliary assembly or mispositioned signaling receptors, which in turn contributes to sensory impairments and ciliopathies. Working alongside the IFT machinery is the BBSome, an octameric protein complex that acts as a critical adaptor for ciliary membrane trafficking. Mutations in BBSome components impair trafficking efficiency, causing IFT proteins and membrane receptors to accumulate abnormally at the ciliary tip, as observed in Bardet-Biedl syndrome. The BBSome comprises multiple subunits with specialized functions. The BBSome is comprised of several essential subunits, such as BBS1, BBS2, BBS7, and BBS9, which create the structural basis of the complex and engage in interactions with cargo proteins associated with the membrane. In contrast, additional components such as BBS4, BBS5, BBS8, and BBS18 contribute to the proper localization of the BBSome at the basal body and support its association with cellular membranes (Klink et al., 2017) body targeting and membrane association (Klink et al., 2017). The structural characterization has shown that the IFT20-IFT38 module within the IFT-B complex interacts with BBS1, BBS2, and BBS9, creating a functional docking interface either at the base of the cilia or along IFT trains (Nakayama et al., 2018). This interface facilitates the regulated transfer of GPCRs and other signaling cargo between the IFT machinery and the BBSome, ensuring precise loading and unloading at the ciliary base and tip (Nozaki et al., 2018). This IFT-BBSome motor coordination is conserved (Sung et al., 2013). In the single-celled alga *Chlamydomonas reinhardtii*, comparable trafficking processes are important for the proper localization and upkeep of bacteriorhodopsin-type rhodopsins within the flagellar membrane, where they play a role in light-driven phototaxis (Awasthi et al., 2016). Nevertheless, the role of IFT20 in the trafficking of channelrhodopsins remains poorly understood, representing a significant gap.

To address this gap, we investigated the role of IFT20 in ciliary trafficking of channelrhodopsin-1 in *C. reinhardtii*. Previous studies suggest that channelrhodopsin-1 relocates between the eyespot and flagella in a light-dependent manner, whereas channelrhodopsin-2 is exclusively localized to the eyespot and basal body under similar conditions. Additionally, IFT20 is known to link the IFT complex to kinesin-II through ATP-dependent interactions with IFT57 and KIF3B (Krock et al., 2008). Building on this framework, we performed a comprehensive bioinformatic, biochemical, and cell-biological assessment. In this study, we focus solely on the IFT20-mediated ciliary distribution of channelrhodopsins (ChR1). Our findings demonstrate that heterologously expressed CrIFT20

undergoes GTP-dependent conformational changes, as evidenced by secondary structure transitions in CD spectroscopy. These results establish CrIFT20 as a conserved molecular adaptor that sequentially couples early trafficking partners, IFT-B, and BBSome-mediated sorting to regulate channelrhodopsin trafficking in *Chlamydomonas cilia*, with implications for ciliary membrane protein transport across ciliated organisms.

2. Materials and methods

2.1 Bioinformatic analysis of IFT20 homologs

The IFT20 protein sequences were obtained from the NCBI (https://www.ncbi.nlm.nih.gov/) and JGI Genome Portal (https://jgi.doe.gov/) by performing pBLAST searches against the non-redundant database. Domain architecture was analyzed using the CDART tool (Geer et al., 2002). The multiple protein sequence homology analysis was performed using the ClustalW (https://www.ebi.ac.uk/jdispatcher/msa/clustalo) program and visualized by BioEdit (http://www.mbio.ncsu.edu/bioedit/bioedit.html). Conserved sequence motifs within IFT20 homologs were detected using the Multiple Expectation Maximization for Motif Elicitation (MEME) Suite (MEME version 5.5.8) (Bailey et al., 2009). Motifs showing strong statistical support (E-value: $1 \times 10^{-}$) were selected for downstream analyses, and their significance was determined based on the associated E-values. An analysis of the secondary structure was performed using the CFSSP (Chou and Fasman Secondary Structure Prediction Server) online tool, available via the ExPASy server. Phylogenetic analysis of IFT20 proteins was performed in MEGA11 (Tamura et al., 2021) using 1000 bootstrap replicates. Pairwise distances were calculated with the JTT model, and initial trees were generated using the Neighbor-Joining and BioNJ methods. These preliminary topologies were then evaluated to identify the tree with the highest log-likelihood score.

2.2 Protein-protein interaction network prediction

IFTs, BBSomes and ancillary protein sequences were obtained from JGI Genome Portal and NCBI database and subjected to protein-protein interaction (PPI) analysis using STRING v11, based on multisource evidences (Szklarczyk et al., 2019). Interaction networks were subsequently visualized using Cytoscape v3.10.3 (Shannon et al., 2003).

2.3 Structural modeling of IFT20 homologs

The tertiary structures of IFT20 homologs were predicted using the AlphaFold Server (https://alphafoldserver.com/welcome). Structural alignments of protein models were performed in PyMOL v3.1 (https://www.pymol.org/). The sequences used in multiple sequence alignment, phylogenetic analysis, and structural superimposition are listed in **Supplementary Table S1**.

2.4 Heterologous expression and affinity purification of recombinant CrIFT20 proteins

The synthesized CrIFT20 coding sequence was sub-cloned into the pET-21a(+) vector and expressed in *E. coli* BL21 (λDE3). An overnight-grown culture was inoculated into 500 mL Terrific Broth medium (TB) containing 100 μg/mL ampicillin. The incubation was carried out at 37 °C, 200 rpm. When the OD was attained in a range of 0.6–0.8, the cells were chilled on ice for 45 min, culture induction was carried out with 0.3 mM IPTG and grown at 16 °C for 48 hours. Cells were harvested (3,500×g, 10 min, 4°C), resuspended in PBS buffer containing lysozyme (0.5 mg/mL) and PMSF (0.2 mM), and lysed by sonication (50% amplitude, 10 s on/off, 10 min). The lysates were subjected to centrifugation (13,000 × g, 60 min, 4 °C) and filtered. Then the supernatant was loaded onto a pre-equilibrated Ni-NTA IMAC column with PBS (150 mM NaCl, 10 mM sodium phosphate, pH 7.2). After binding and washing, His-tagged CrIFT20 was eluted with 250 mM imidazole. The protein samples were subjected to electrophoresis on a 12% SDS–PAGE gel and then electroblotted onto a nitrocellulose membrane at 4 °C (350 mA, 90 min). Blocking was carried out with 5% milk in PBST and incubated with anti-His primary antibodies (1:5000), followed by HRP-conjugated secondary antibodies (1:5000). Signal detection was carried out using enhanced chemiluminescence (ECL). The workflow for recombinant protein expression and purification was adapted from established protocols (Wang et al., 2018).

2.5 Fluorescence spectroscopy of recombinant CrIFT20

Intrinsic tyrosine fluorescence measurements of recombinant CrIFT20 (3.5 μM) were performed using a Varian Cary Eclipse fluorescence spectrophotometer (Agilent Technologies). The excitation of samples was carried out at 275 nm (5 nm excitation slit width), and emission spectra were recorded from 290-400 nm (5 nm emission slit width) at room temperature. GTP (Sigma-Aldrich) was diluted in the reaction buffer (50 mM Tris-HCl, pH 8). For GTP-binding assay, CrIFT20 concentration of 3.5 μM was used. Buffer blank fluorescence was subtracted from all spectra, and data were analyzed by standard methods.

2.6 Circular dichroism spectroscopy recombinant CrIFT20

Purified recombinant CrIFT20 was analyzed by far-UV circular dichroism (190-260 nm), using 20 mM Tris-HCl, pH 8, as the buffer control at room temperature. CD spectra were monitored following the addition of increasing GTP concentrations. Measurements were performed on a Jasco J-815 spectrometer (Jasco, Tokyo, Japan) containing a 250 W xenon lamp, using a 1 mm path-length cuvette, a scanning speed of 50 nm per min, and a bandwidth of 0.5 nm. Each individual spectrum represents the mean of five scans, and buffer background spectra were subtracted from all datasets.

2.7 Chlamydomonas culture, protein extraction, and immunoblotting

Chlamydomonas reinhardtii wild-type (CC-125) used in this study were obtained from the Chlamydomonas Resource Center (https://www.chlamycollection.org/). Wild-type strain was cultured in standard Tris-acetate-phosphate (TAP) medium. Culture was propagated at 22 °C using a light/dark pattern where the cells were exposed to light for 14 h, followed by dark exposure for 10 h, with continuous shaking at 110 rpm (Catalan, 2025). Culture was collected at an optical density (OD□□□) of approximately 0.6 by centrifugation at 5000 rpm for 10 min. The resuspension of the cell pellet was done in 1XPBS having 0.1% protease inhibitor cocktail (PIC). Lysis was performed by sonication at 30% amplitude with 8-second on/off cycles. After carrying out centrifugation at 13,000 rpm for 15 min, the clarified lysate was collected, mixed with Laemmli buffer, and heated at 65□°C for 30 min. Proteins were separated on an SDS-PAGE and transferred to the nitrocellulose (NC) membrane. Incubation with the diluted primary antibody (1:1000) in 1X PBS was performed for 1 h. The membrane was washed with PBST, followed by incubation with HRP-conjugated secondary antibody (1:1000) (Sigma Aldrich, Missouri, United States) for 1 h. Post washing with PBST, the protein bands were captured using standard laboratory protocols on the X-ray film.

2.8 Cellular co-immunolocalization of CrIFT20 and ChR1

A culture grown to an OD□□□ of ~0.6 was used for the assay. Coverslips were washed and layered with 0.1 mg/mL poly-L-lysine (Sigma-Aldrich), and algal cells were seeded onto the coated coverslips and incubated at room temperature for 15 min. Fixation was done with a freshly prepared 3.7% paraformaldehyde in PBS for 15 min. Following fixation, coverslips were transferred to chilled ethanol at -20□°C for 20 min. Post fixation and permeabilization,

cells were rehydrated in PBS having 250 mM NaCl, then washed with PBS containing 0.5% Triton X-100 (PBST), and placed in blocking buffer (1X PBS and 5% BSA) for 1 h at room temperature. The permeabilized cells were incubated overnight at 4 °C with freshly diluted primary antibodies: CrIFT20 (1:250) and ChR1-Ct (1:250). Again, after washing with PBST and PBS, the coverslips were incubated at 37 °C for 1 h with Alexa Fluor-conjugated secondary antibodies (1:1000) (anti-goat Alexa-488 and anti-rabbit Alexa-546; Invitrogen, USA). Following additional washes with PBST and PBS, the coverslips were mounted onto glass slides using SlowFade® Gold antifade reagent (Molecular Probes, Invitrogen, USA) (Lechtreck et al., 2013). Samples were imaged using an Olympus Fluoview 1000 confocal microscope. The details of antibodies used in this study is mentioned in **Supplementary Table S2**.

2.9 Co-immunoprecipitation

Chlamydomonas reinhardtii cells were grown under a 14 h light/10 hr dark cycle and collected by centrifugation (5000 rpm, 10 min). Cell pellets were resuspended in 50 mM Tris-Cl, pH 8, buffer containing 1% NP-40, 1 mM PMSF, 1 mM sodium orthovanadate, and 0.1% SDS, and a cocktail of protease inhibitors (Sigma-Aldrich). The lysates were sonicated and precleared by incubation with preimmune serum and a protein A/G bead slurry for 2 hr at 4 °C with gentle rotation. The separation of the beads was undertaken by centrifuging at 13,300 rpm at 4°C for 10 min. The procured supernatant was subjected to co-immunoprecipitation studies. For immunoprecipitation, 1 mL of the pre-cleared lysate was kept overnight at 4 °C with rotation using pre-immune serum (negative control) and the specific primary antibody. Next day, incubation of the lysate with Protein A-Sepharose beads slurry was carried out for 2 h at 4°C. Immune complexes were centrufuged at low speed, and washed thrice with 1× PBS. The elution was undertaken with 0.1 M glycine (pH 2.8). The eluted samples were prepared using 4× Laemmli sample buffer abnd heated at 65 °C for 30 min. The bands were separated via SDS-PAGE, and further analyzed by immunoblotting.

3. Results

3.1 Phylogenetic and sequence homology analysis reveal a conserved functional core of IFT20 in ciliary trafficking

Comparative sequence homology and secondary structure analyses of IFT20 homologs revealed that the C-terminal coiled-coil domain is highly conserved, consistent with its

established role in intraflagellar transport complex assembly (Lechtreck et al., 2022). In contrast, the N-terminal region exhibits marked sequence variation and comprises β-strands linked by a flexible loop **(Fig. 1A)**, a configuration that likely contributes to species-specific modulation of IFT20 function and its interactions within the ciliary transport system. Motif analysis further identified three discrete, conserved sequence elements across homologs, detected through expectation-maximization algorithms that quantify motif enrichment and position-specific conservation **(Fig. 1A)**. These motifs define critical interaction interfaces required for engaging intraflagellar transport components or adaptor proteins involved in ciliary trafficking. Notably, a conserved YEFI motif (Y111–E118–F124–I129) emerged as a key determinant mediating IFT20's interaction with the WD40 domain of the autophagy-related protein ATG16 (Boukhalfa et al., 2021). Phylogenetic reconstruction further supports this pattern of structural constraint and molecular divergence. Chlorophyte sequences create a well-supported clade, suggesting that the IFT20 structure in algae has stayed consistent among flagellated green lineages **(Fig. 1B)**. Streptophyte homologs, including those from early land plants, form a distinct cluster, consistent with functional divergence associated with terrestrial adaptation. Oomycete IFT20 proteins group together in a well-supported (bootstrap 100), lineage-specific clade, reflecting the adaptation of the IFT pathway within this heterokont group. Metazoan homologs form a separate basal branch, consistent with an early evolutionary split of the ciliary transport machinery in animals. Among all groups, Chlorophyta exhibits the highest retention of the ancestral IFT20 configuration **(Fig. 1B)**, consistent with the conserved molecular features required for ciliary transport in *Chlamydomonas*. Together, the combined sequence alignment and phylogenetic evidence demonstrate that IFT20 retains a highly conserved core essential for its canonical role in IFT-B assembly, while the flanking regions accumulate lineage-specific variability that may support specialized regulatory functions. The close clustering of *Chlamydomonas* with other chlorophytes supports the use of *C. reinhardtii* as a tractable model for studying ancestral features of IFT20-mediated ciliary trafficking.

3.2 A conserved coiled-coil module stabilizes the IFT20 structure

Recombinant CrIFT20 was heterologously expressed in *E. coli*. Bacterial cultures carrying the expression construct were lysed, and the clarified lysates were purified using immobilized metal affinity chromatography (IMAC), which enabled the selective enrichment of His-tagged CrIFT20. The purified fractions were resolved on SDS-PAGE. A prominent band of

~15 kDa was observed **(Fig. 2A)**, matching the predicted size of full-length CrIFT20. The gel was used for western blotting with an anti-His antibody. Elution fractions E1 to E5 displayed a ~15 kDa signal, confirming that the purified protein corresponds to the His-tagged CrIFT20 **(Fig. 2B)**. Integrative structural modelling coupled with biophysical validation revealed that IFT20 proteins maintain a deeply conserved architectural core across eukaryotes. Cross-species superposition of predicted IFT20 protein structures demonstrated near-perfect alignment of the C-terminal coiled-coil region **(Fig. 2C)**. Despite substantial divergence within the N-terminal segment, consistent with its role as a rigid interaction platform required for stable incorporation into the IFT-B scaffold and for maintaining IFT train architecture. Bioinformatic analysis of quantitative secondary-structure across IFT20's homologs further demonstrated a uniformly elevated helical content (76–93%) **(Supplementary Table S3)**. In contrast, β-strand and turn content varied in a lineage-dependent manner, suggesting that structural plasticity is restricted to peripheral regions not directly involved in IFT-B complex assembly. Together, these data indicate that IFT20 possesses a highly conserved helical core that is evolutionarily constrained to preserve its architectural and scaffolding functions within ciliary transport systems, while allowing modular divergence in non-core segments that may underlie lineage-specific tuning of IFT20 protein dynamics (Finetti et al., 2022).

3.3 IFT20 binds to GTP in a concentration dependent manner

To define the molecular machinery involved in channelrhodopsin-1 (ChR1) trafficking within the cilia of *C. reinhardtii*, we first mapped the core and ancillary flagellar proteins that co-associate with ChR1. This analysis was performed using a curated protein-protein interaction (PPI) network specific to *C. reinhardtii* **(Fig. S1A)**. This comprehensive PPI network integrates four major curated clusters, defining vesicle-mediated transport proteins, intraflagellar transport (IFT), and BBSomes components. We next identified the highest-confidence interactors **(Fig. S1B)**. The resulting top-interacting protein network revealed a densely interconnected module comprising canonical IFT-B components (IFT57, IFT81, IFT88, IFT172, IFT74), membrane-trafficking GTPases (Arl3, RABG1, RABA1, YKT6, ARFA1), and BBSome subunits (BBS1, BBS5, BBS7) (Kiral et al., 2018; Kobayashi et al., 2021; Petriman et al., 2022. Lechtreck et al., 2009). High-ranked nodes corresponded to proteins with established roles in ciliary membrane trafficking. These findings support the central positioning of IFT20 at the interface between IFT-B assembly and vesicle-associated

transport. To evaluate how CrIFT20 couples with small GTPase for ciliary trafficking of proteins, coordination between Arf-dependent vesicle formation and IFT-B handoff, linking general membrane trafficking with specialized ciliary transport. The schematic representation of the construct developed in this study for the recombinant expression of CrIFT20 has been depicted in **Fig. S2**. During the *in vitro* study, the CrIFT20 was biophysically characterised using fluorescence spectroscopy and far-UV CD spectroscopy **(Fig. 3)**. Intrinsic tyrosine fluorescence analysis revealed a single broad emission maximum at 304 nm. The purified CrIFT20 was spectroscopically analyzed after the sequential addition of GTP. Changes in the fluorescence intensity was observed upon binding with increasing concentrations of GTP **(Fig. 3A)**. A positive peak at 195 nm for the recombinant CrIFT20 protein confirmed its alpha helical structure. A change in the CD spectrum was recorded upon increasing the concentrations of GTP **(Fig. 3B)**. This study confirmed that the addition of GTP in a concentration-dependent manner induced conformational changes in the CrIFT20 that resulted in fluorescence quenching and shift in CD spectra.

3.4 Cellular co-localization of IFT20 and ChR1 in Chlamydomonas reinhardtii

IFT20 is a key adaptor protein involved in the sorting of ciliary membrane proteins, dynamically shuttling between the Golgi complex, basal body, and cilium. For understanding the molecular and cellular function of IFT20 in ciliary membrane protein trafficking in *C. reinhardtii*. We performed immunoblotting and immunolocalization of wild-type *C. reinhardtii* CC-125 strain, which revealed a prominent ~15 kDa band with anti-CrIFT20 antibody, corresponding to endogenous CrIFT20 **(Fig. S3 and Fig. S4)**. Immunofluorescence detection using a CrIFT20-specific antibody in the wild-type *C. reinhardtii* strain CC125, which revealed that IFT20 is prominently localized throughout the cilia (**Fig. S4)**. The staining appears as punctate green fluorescence throughout the cilia. Co-immunostaining with ChR1 demonstrated significant spatial overlap with IFT20 in the merged fluorescence images, indicating that IFT20 and ChR1 can be co-localized directly/indirectly in the cilia **(Fig. 4A)**. The determination of an association of ChR1 with IFT20, a co-immunoprecipitation experiment was performed using anti-ChR1Ct and anti-IFT20 antibodies from *C. reinhardtii* Total Cell Lysate (CrTCL). The detection of IFT20 in the immunoprecipitant of ChR1-Ct was undertaken via an anti-IFT20 antibody **(Fig. 4B)**. Using a similar strategy, in the inverse blot, ChR1 was blotted in the IFT20 immunoprecipitant **(Fig. 4C)**. A unique observation was recorded which showed that the subcellular localization of

IFT20 in the eyespot. However, the exact mechanism for the above observation still needs to be elucidated. This functional interaction, in which IFT20 likely facilitates the targeted trafficking and proper localization of photoreceptors, such as ChR1, within the cilia of *C. reinhardtii*. These results provide cellular biochemical evidence that CrIFT20 physically interacts with its ciliary membrane cargo ChR1, supporting its role as a ciliary membrane trafficking.

4. Conclusions

The current work focusses on the identification of *C. reinhardtii* IIFT20 as an adapter protein that guides the trafficking of channelrhodopsin-1 in the cilia. The CrIFT20 was found to contain a conserved coiled-coil domain that is crucial for IFT-B complex assembly. It also directs the trafficking of membrane proteins in the cilia. The recombinant expression of CrIFT20 was targeted in the *E. coli* cells, whose biophysical characterization highlighted its alpha-helical structure. The subcellular localization studies showed that IFT20 co-localizes with the channelrhodopsin-1, facilitating the targeted transport of receptors to the ciliary membrane.

CRediT authorship contribution statement

Suneel Kateriya: Conceptualisation, Data curation and Methodology, Supervision, Validation, Funding acquisition. **Alka Kumari:** Formal analysis, Investigation, Writing-original draft, Methodology. **Shilpa Mohanty:** Methodology, Investigation, Writing-review and editing. **Snigdha Samanta:** Investigation.

Declaration of Competing Interest

The authors declare no conflict of interest.

Funding

We are thankful to ANRF/SERB, Government of India for granting EEQ/2023/000398 research project.

Acknowledgements

Alka Kumari is the recipient of the Senior Research Fellowship from UGC (JRF), Govt. of India.

Data availability

The data is available on request.

References

1. Awasthi, M., Ranjan, P., Sharma, K., Veetil, S. K., & Kateriya, S. (2016). The trafficking of bacterial type rhodopsins into the *Chlamydomonas* eyespot and flagella is IFT mediated. *Scientific Reports*, *6*(1), 34646.
2. Bailey, T. L., Boden, M., Buske, F. A., Frith, M., Grant, C. E., Clementi, L., ... & Noble, W. S. (2009). MEME SUITE: tools for motif discovery and searching. *Nucleic acids research*, *37*(suppl_2), W202-W208.
3. Baker, S. A., Freeman, K., Luby-Phelps, K., Pazour, G. J., & Besharse, J. C. (2003). IFT20 links kinesin II with a mammalian intraflagellar transport complex that is conserved in motile flagella and sensory cilia. *Journal of Biological Chemistry*, *278*(36), 34211-34218.
4. Blacque, O. E., Scheidel, N., & Kuhns, S. (2018). Rab GTPases in cilium formation and function. *Small GTPases*, *9*(1-2), 76-94.
5. Boegholm, N., Petriman, N. A., Loureiro□López, M., Wang, J., Vela, M. I. S., Liu, B., ... & Lorentzen, E. (2023). The IFT81□IFT74 complex acts as an unconventional RabL2 GTPase□activating protein during intraflagellar transport. *The EMBO journal*, *42*(18), e111807.
6. Boukhalfa, A., Roccio, F., Dupont, N., Codogno, P., & Morel, E. (2021). The autophagy protein ATG16L1 cooperates with IFT20 and INPP5E to regulate the turnover of phosphoinositides at the primary cilium. *Cell Reports*, *35*(4).
7. Deretic, D. *Crosstalk of Arf and Rab GTPases en route to cilia*. *Small GTPases 2013; 4: 70-7; PMID: 23567335*.
8. Deretic, D., Lorentzen, E., & Fresquez, T. (2021). The ins and outs of the Arf4-based ciliary membrane-targeting complex. *Small GTPases*, *12*(1), 1-12.
9. Deretic, D., Williams, A. H., Ransom, N., Morel, V., Hargrave, P. A., & Arendt, A. (2005). Rhodopsin C terminus, the site of mutations causing retinal disease, regulates trafficking by binding to ADP-ribosylation factor 4 (ARF4). *Proceedings of the National Academy of Sciences*, *102*(9), 3301-3306.

10. Evans, R., O'Neill, M., Pritzel, A., Antropova, N., Senior, A., Green, T., ... & Hassabis, D. (2021). Protein complex prediction with AlphaFold-Multimer. *biorxiv*, 2021-10.
11. Finetti, F., Onnis, A., & Baldari, C. T. (2022). IFT20: an eclectic regulator of cellular processes beyond intraflagellar transport. *International Journal of Molecular Sciences*, *23*(20), 12147.
12. Fliegauf, M., Benzing, T., & Omran, H. (2007). When cilia go bad: cilia defects and ciliopathies. *Nature reviews Molecular cell biology*, *8*(11), 880-893.
13. Follit, J. A., San Agustin, J. T., Xu, F., Jonassen, J. A., Samtani, R., Lo, C. W., & Pazour, G. J. (2008). The Golgin GMAP210/TRIP11 anchors IFT20 to the Golgi complex. *PLoS genetics*, *4*(12), e1000315.
14. Geer, L. Y., Domrachev, M., Lipman, D. J., & Bryant, S. H. (2002). CDART: protein homology by domain architecture. *Genome research*, *12*(10), 1619-1623.
15. Hanke-Gogokhia, C., Wu, Z., Gerstner, C. D., Frederick, J. M., Zhang, H., & Baehr, W. (2016). Arf-like protein 3 (ARL3) regulates protein trafficking and ciliogenesis in mouse photoreceptors. *Journal of Biological Chemistry*, *291*(13), 7142-7155.
16. Jiang, M., Palicharla, V. R., Miller, D., Hwang, S. H., Zhu, H., Hixson, P., ... & Sun, J. (2023). Human IFT-A complex structures provide molecular insights into ciliary transport. *Cell research*, *33*(4), 288-298.
17. Kiral, F. R., Kohrs, F. E., Jin, E. J., & Hiesinger, P. R. (2018). Rab GTPases and membrane trafficking in neurodegeneration. *Current Biology*, *28*(8), R471-R486.
18. Klink, B. U., Zent, E., Juneja, P., Kuhlee, A., Raunser, S., & Wittinghofer, A. (2017). A recombinant BBSome core complex and how it interacts with ciliary cargo. *Elife*, *6*, e27434.
19. Kobayashi, T., Ishida, Y., Hirano, T., Katoh, Y., & Nakayama, K. (2021). Cooperation of the IFT-A complex with the IFT-B complex is required for ciliary retrograde protein trafficking and GPCR import. *Molecular biology of the cell*, *32*(1), 45-56.
20. Krock, B. L., & Perkins, B. D. (2008). The intraflagellar transport protein IFT57 is required for cilia maintenance and regulates IFT-particle–kinesin-II dissociation in vertebrate photoreceptors. *Journal of cell science*, *121*(11), 1907-1915.
21. Lechtreck, K. (2022). Cargo adapters expand the transport range of intraflagellar transport. *Journal of cell science*, *135*(24), jcs260408.
22. Lechtreck, K. F. (2013). In vivo imaging of IFT in *Chlamydomonas* flagella. In *Methods in enzymology* (Vol. 524, pp. 265-284). Academic Press.

23. Lechtreck, K. F. (2015). IFT–cargo interactions and protein transport in cilia. *Trends in biochemical sciences*, *40*(12), 765-778.
24. Lechtreck, K. F., Johnson, E. C., Sakai, T., Cochran, D., Ballif, B. A., Rush, J., ... & Witman, G. B. (2009). The *Chlamydomonas reinhardtii* BBSome is an IFT cargo required for export of specific signaling proteins from flagella. *Journal of Cell Biology*, *187*(7), 1117-1132.
25. Leroux, M. R. (2007). Taking vesicular transport to the cilium. *Cell*, *129*(6), 1041-1043.
26. Masek, M., Etard, C., Hofmann, C., Hülsmeier, A. J., Zang, J., Takamiya, M., ... & Bachmann-Gagescu, R. (2022). Loss of the Bardet-Biedl protein Bbs1 alters photoreceptor outer segment protein and lipid composition. *Nature Communications*, *13*(1), 1282.
27. Mill, P., Christensen, S. T., & Pedersen, L. B. (2023). Primary cilia as dynamic and diverse signalling hubs in development and disease. *Nature Reviews Genetics*, *24*(7), 421-441.
28. Morthorst, S. K., Christensen, S. T., & Pedersen, L. B. (2018). Regulation of ciliary membrane protein trafficking and signalling by kinesin motor proteins. *The FEBS journal*, *285*(24), 4535-4564.
29. Nakayama, K., & Katoh, Y. (2018). Ciliary protein trafficking mediated by IFT and BBSome complexes with the aid of kinesin-2 and dynein-2 motors. *The journal of biochemistry*, *163*(3), 155-164.
30. Nozaki, S., Katoh, Y., Kobayashi, T., & Nakayama, K. (2018). BBS1 is involved in retrograde trafficking of ciliary GPCRs in the context of the BBSome complex. *PLoS One*, *13*(3), e0195005.
31. Pazour, G. J., Baker, S. A., Deane, J. A., Cole, D. G., Dickert, B. L., Rosenbaum, J. L., ... & Besharse, J. C. (2002). The intraflagellar transport protein, IFT88, is essential for vertebrate photoreceptor assembly and maintenance. *The Journal of cell biology*, *157*(1), 103-114.
32. Petriman, N. A., Loureiro□López, M., Taschner, M., Zacharia, N. K., Georgieva, M. M., Boegholm, N., ... & Lorentzen, E. (2022). Biochemically validated structural model of the 15□subunit intraflagellar transport complex IFT□B. *The EMBO journal*, *41*(24), e112440.
33. Reiter, J. F., & Leroux, M. R. (2017). Genes and molecular pathways underpinning ciliopathies. *Nature reviews Molecular cell biology*, *18*(9), 533-547.

34. Saha, I., Insinna, C., & Westlake, C. J. (2024). Rab11-Rab8 cascade dynamics in primary cilia and membrane tubules. *Cell reports*, *43*(11).
35. Satir, P., Pedersen, L. B., & Christensen, S. T. (2010). The primary cilium at a glance. *Journal of cell science*, *123*(4), 499-503.
36. Satir, P., Pedersen, L. B., & Christensen, S. T. (2010). The primary cilium at a glance. *Journal of cell science*, *123*(4), 499-503.
37. Shannon, P., Markiel, A., Ozier, O., Baliga, N. S., Wang, J. T., Ramage, D., ... & Ideker, T. (2003). Cytoscape: a software environment for integrated models of biomolecular interaction networks. *Genome research*, *13*(11), 2498-2504.
38. Singh, S. K., Gui, M., Koh, F., Yip, M. C., & Brown, A. (2020). Structure and activation mechanism of the BBSome membrane protein trafficking complex. *elife*, *9*, e53322.
39. Stoetzel, C., Bär, S., De Craene, J. O., Scheidecker, S., Etard, C., Chicher, J., ... & Dollfus, H. (2016). A mutation in VPS15 (PIK3R4) causes a ciliopathy and affects IFT20 release from the cis-Golgi. *Nature communications*, *7*(1), 13586.
40. Sung, C. H., & Leroux, M. R. (2013). The roles of evolutionarily conserved functional modules in cilia-related trafficking. *Nature cell biology*, *15*(12), 1387-1397.
41. Szklarczyk, D., Gable, A. L., Lyon, D., Junge, A., Wyder, S., Huerta-Cepas, J., ... & Mering, C. V. (2019). STRING v11: protein–protein association networks with increased coverage, supporting functional discovery in genome-wide experimental datasets. *Nucleic acids research*, *47*(D1), D607-D613.
42. Takei, R., Katoh, Y., & Nakayama, K. (2018). Robust interaction of IFT70 with IFT52–IFT88 in the IFT-B complex is required for ciliogenesis. *Biology open*, *7*(5), bio033241.
43. Tamura, K., Stecher, G., & Kumar, S. (2021). MEGA11: molecular evolutionary genetics analysis version 11. *Molecular biology and evolution*, *38*(7), 3022-3027.
44. Tasaki, K., Zhou, Z., Ishida, Y., Katoh, Y., & Nakayama, K. (2023). Compound heterozygous IFT81 variations in a skeletal ciliopathy patient cause Bardet–Biedl syndrome-like ciliary defects. *Human Molecular Genetics*, *32*(19), 2887-2900.
45. Taschner, M., Weber, K., Mourão, A., Vetter, M., Awasthi, M., Stiegler, M., ... & Lorentzen, E. (2016). Intraflagellar transport proteins 172, 80, 57, 54, 38, and 20 form a stable tubulin□binding IFT□B2 complex. *The EMBO journal*, *35*(7), 773-790.

46. Wang, J., Fresquez, T., Kandachar, V., & Deretic, D. (2017). The Arf GEF GBF1 and Arf4 synergize with the sensory receptor cargo, rhodopsin, to regulate ciliary membrane trafficking. *Journal of cell science*, *130*(23), 3975-3987.
47. Wang, Q., Pan, J., & Snell, W. J. (2006). Intraflagellar transport particles participate directly in cilium-generated signaling in *Chlamydomonas*. *Cell*, *125*(3), 549-562.
48. Wang, Q., Taschner, M., Ganzinger, K. A., Kelley, C., Villasenor, A., Heymann, M., ... & Mizuno, N. (2018). Membrane association and remodeling by intraflagellar transport protein IFT172. *Nature Communications*, *9*(1), 4684.
49. Wang, Q., Taschner, M., Ganzinger, K. A., Kelley, C., Villasenor, A., Heymann, M., ... & Mizuno, N. (2018). Membrane association and remodeling by intraflagellar transport protein IFT172. *Nature Communications*, *9*(1), 4684.
50. Ward, H. H., Brown-Glaberman, U., Wang, J., Morita, Y., Alper, S. L., Bedrick, E. J., ... & Wandinger-Ness, A. (2011). A conserved signal and GTPase complex are required for the ciliary transport of polycystin-1. *Molecular biology of the cell*, *22*(18), 3289-3305.
51. Wingfield, J. L., Lechtreck, K. F., & Lorentzen, E. (2018). Trafficking of ciliary membrane proteins by the intraflagellar transport/BBSome machinery. *Essays in biochemistry*, *62*(6), 753-763.
52. Ye, F., Nager, A. R., & Nachury, M. V. (2018). BBSome trains remove activated GPCRs from cilia by enabling passage through the transition zone. *Journal of Cell Biology*, *217*(5), 1847-1868.

Figures:

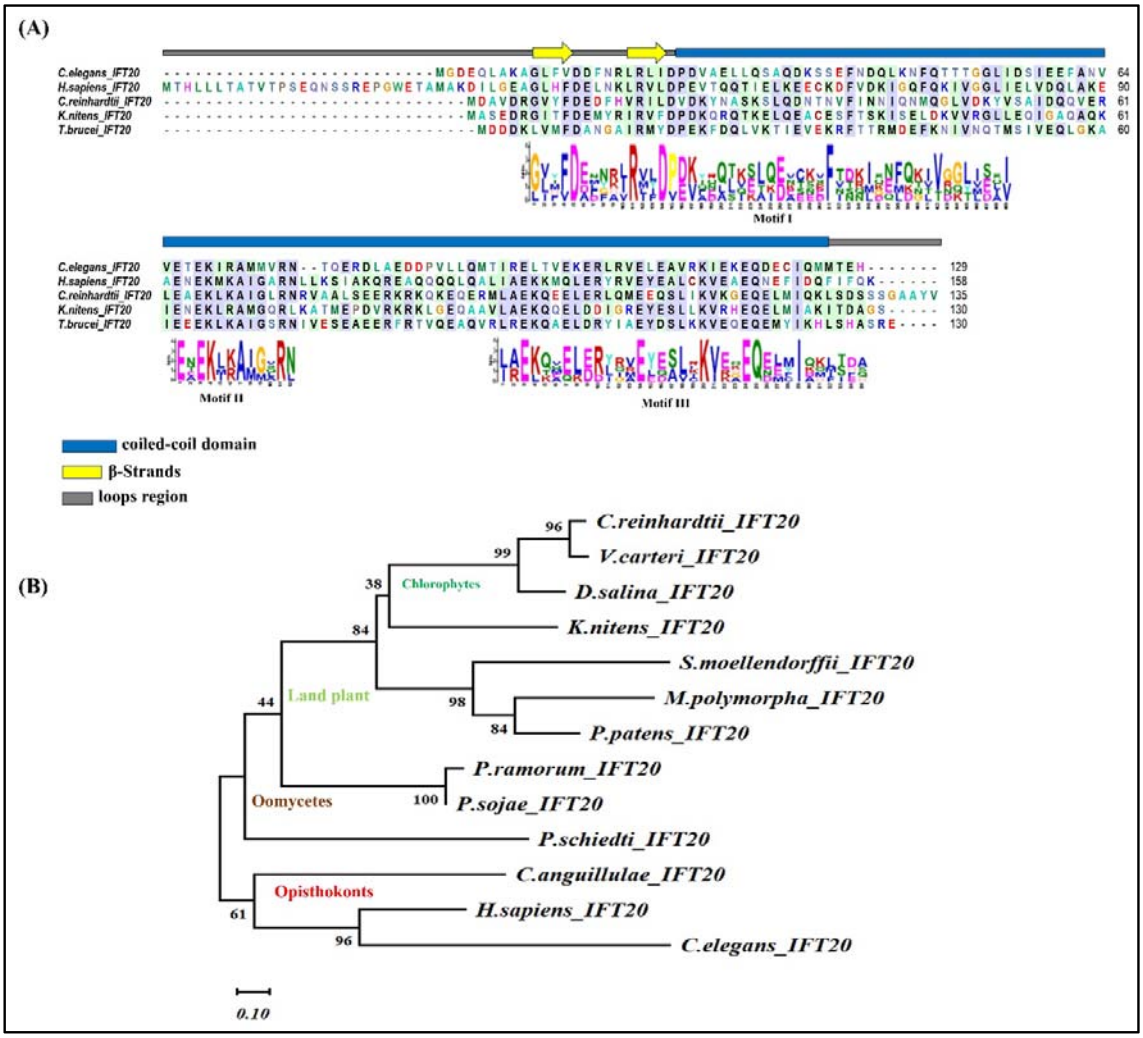

Fig. 1: Sequence conservation and evolutionary relationships of IFT20 homologs. **(A)** Multiple sequence alignment of IFT20 protein sequences from diverse organisms. Conserved residues are highlighted by blue color shading. The alignment highlights strong conservation

across the IFT20 sequences. A schematic representation of the predicted secondary structural elements is shown above the alignment: α-helices (blue bars), β-strands (yellow arrows), and loop regions (grey), indicating structural conservation. MEME (Multiple Expectation Maximization for Motif Elicitation) finds three discrete motif regions. The height of each letter reflects the conservation of residue. *(H. sapiens = Homo sapiens, T. brucei = Trypanosoma brucei, C. reinhardtii = Chlamydomonas reinhardtii, K. nitens = Klebsormidium nitens, C. elegans = Caenorhabditis elegans*. **(B)** The IFT20 protein sequences were aligned using ClustalW in MEGA11. The Maximum likelihood method and the Jonas-Taylor-Thorton model were employed for analysis of the tree with 1000 bootstrap replicates. The evolutionary analyses were carried out using MEGA 11 software.

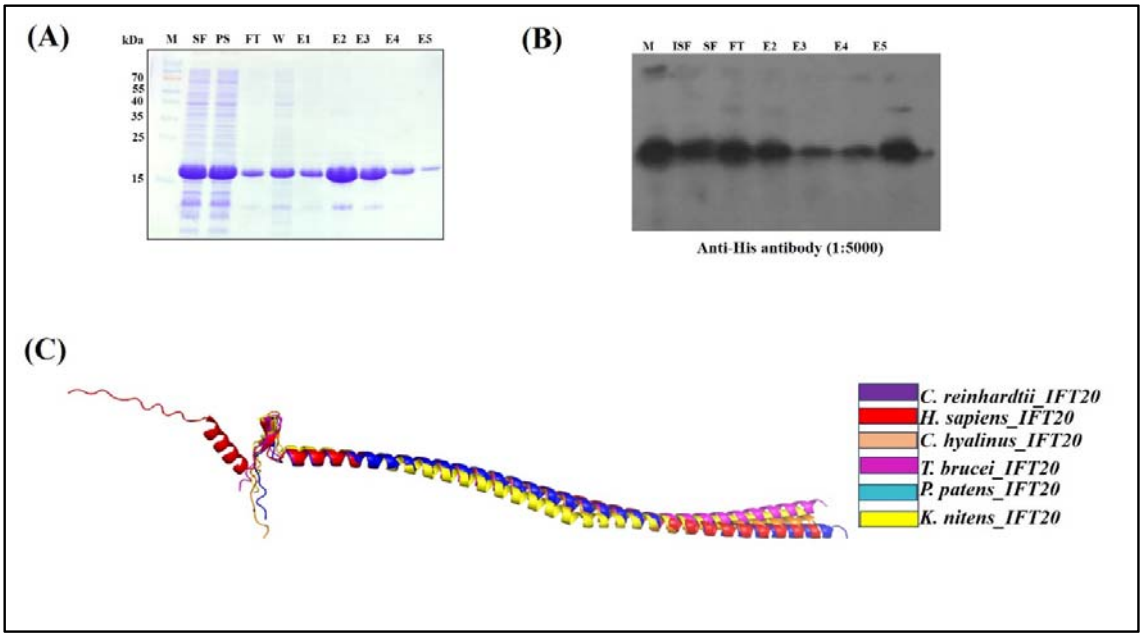

Fig. 2: Structural comparison and recombinant expression of CrIFT20. **(A-B)** SDS-PAGE and western blot analysis of purified CrIFT20 using anti-IFT20 antibody (1:5000). Lane M: protein marker; PS: parent sample; W: wash; ISF: insoluble fraction; SF: soluble fraction; FT: flow through; E1-E5: elution fractions. The recombinant IFT20 protein is detected at ~15 kDa. **(C)** Structural superposition of IFT20 sequences from *Chlamydomonas reinhardtii*, *Homo sapiens*, *Chlamydomonas hyalinus*, *Trypanosoma brucei*, *Physcomitrella patens*, and *Klebsormidium nitens*, color-coded by species.

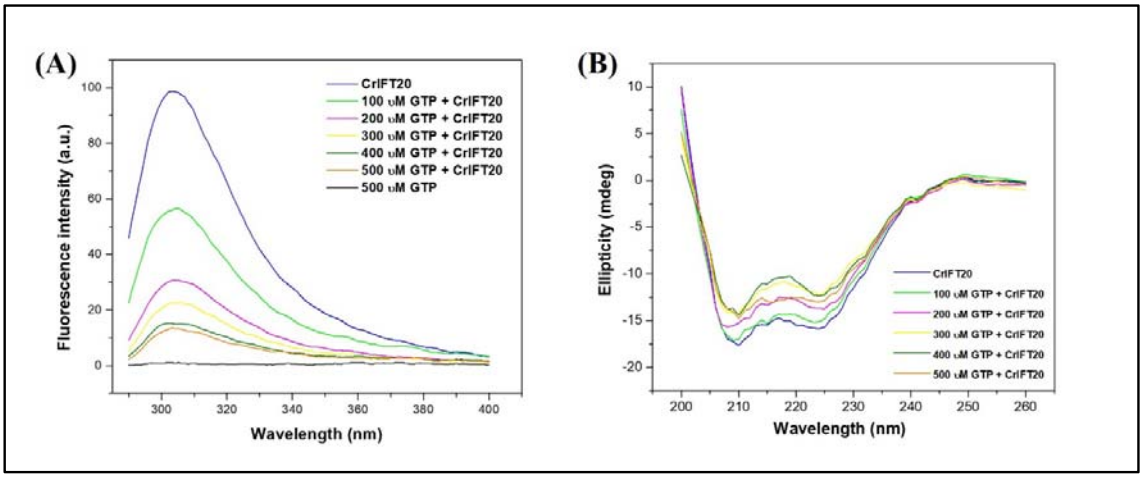

Fig. 3: Molecular docking and GTP-dependent spectroscopic characterization of recombinant CrIFT20. **(A)** Intrinsic fluorescence spectroscopy of recombinant CrIFT20 with increasing GTP concentrations indicating GTP-dependent changes in the local environment of aromatic residues. **(B)** Circular dichroism (CD) spectra of recombinant CrIFT20 under identical GTP concentration showing alterations in α-helical secondary-structure signatures. (GTP - Guanosine Triphosphate)

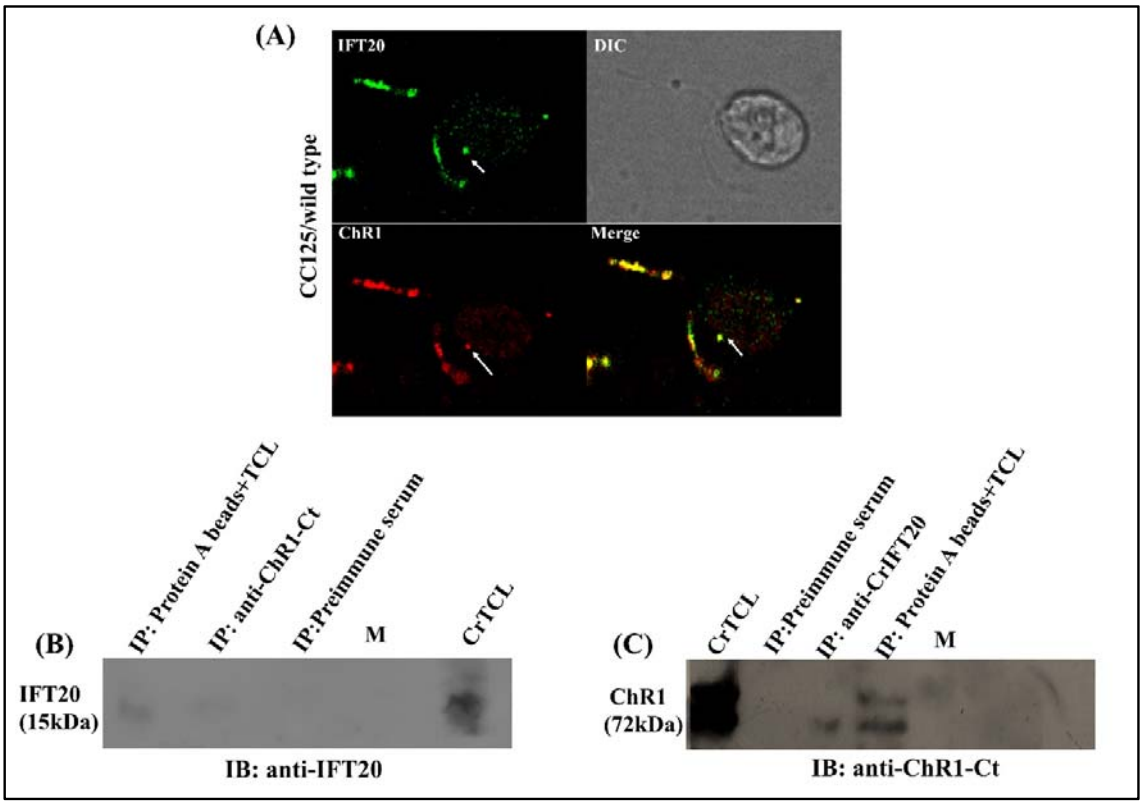

Fig. 4: Co-localization of CrIFT20 with CrChR1 in *Chlamydomonas* wild type CC125. **(A)** Immunofluorescence staining of wild-type *Chlamydomonas reinhardtii* (CC125) showing Differential interference contrast (DIC) image with two intact flagella with the cell body, CrIFT20 immunostaining (green), CrChR1 immunostaining (red), and merged channels. CrIFT20 and ChR1 puncta are both visible within the cilia, with significant spatial overlap in the merged image (yellow). **(B-C)** Immunoprecipitation (IP) of IFT20 and Chr1 using anti-IFT20 and ChR1-Ct antibody followed by immunoblotting (IB) with ChR1-Ct and IFT20 antibody. Protein bands of 72kDa represent ChR1 and 18kDa represent IFT20. IP with pre-immune serum served as negative control. (PIS = pre-immune serum).